

Vesicle Hydrogels Formed from the Perfluorononanoic Acid/Tetradecyl Dimethylaminoxide Oxide System

Juan Zhang,* Ping Liu, Yuan Gao, Qichao Lv, Denglai Wu, Yi Tian, and Jigui Tang



Cite This: *ACS Omega* 2024, 9, 27509–27516



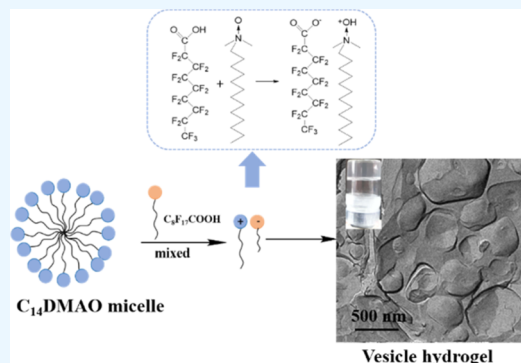
Read Online

ACCESS |

Metrics & More

Article Recommendations

ABSTRACT: Vesicle hydrogels are supramolecular structures formed by the self-assembly of surfactant molecules in solution, which have great application prospects. The phase behavior of perfluorononanoic acid ($C_8F_{17}COOH$) and an amphoteric hydrocarbon surfactant, tetradecyl dimethylaminoxide ($C_{14}DMAO$), in an aqueous solution has been studied. By changing the mixing ratio and concentration of $C_8F_{17}COOH$ and $C_{14}DMAO$, the phase diagram of the system was drawn, and interestingly, a hydrogel composed of polyhedral and spherical vesicles was successfully constructed. The formation mechanism of the polyhedral and spherical vesicle hydrogel was studied by differential scanning calorimetry (DSC), small-angle X-ray diffraction (XRD), wide-angle X-ray scattering (WAXS), and 1H nuclear magnetic resonance (1H NMR) measurements, and the rheological properties and influencing factors of the hydrogel were systematically investigated. The formation of the vesicle hydrogels in this system was considered to be caused by the “cocrystallization” of two surfactant molecular chains.



INTRODUCTION

In recent years, as an attractive, practical, and bottom-up approach, molecular self-assembly has been used to prepare structurally well-defined and functional materials.^{1–4} Especially, hydrogels formed from surfactant self-assembly have drawn much attention due to their low toxicity, multiscale, multilevel, and multistructure.^{5–7} Under certain conditions, vesicles can form hydrogels that retain the properties of both vesicles and gels and therefore show some unique advantages.^{8,9} For instance, researchers have used vesicle hydrogels for drug release and found that the shear-thinning property of the vesicle hydrogel helped these gels become easier to be injected into specific sites, and the drugs encapsulated in the vesicle interior could be released at the local site for a longer time.¹⁰

The research of surfactant vesicle hydrogels has taken decades.^{11–13} Different from the traditional hydrogels with a “three-dimensional” network structure, the one-dimensional structure characteristics of vesicles make it difficult for them to form hydrogels. Usually, researchers must take certain measures to obtain vesicle hydrogels. Hoffmann et al. prepared a vesicle gel phase with sodium oleate and cosurfactant hexyl alcohol in an aqueous solution and found that the formation of vesicle gel must meet two conditions: one was to form monodisperse monolayer vesicles, and the other was that monolayer vesicles must reach a certain density.¹⁴ Besides, the formation process of monodisperse vesicle gel and the relationship between the cosurfactant and surfactant chain length ratio and the concentration ratio of the surfactant and

cosurfactant were proposed, and the phase structure transformation of gel was discussed, which laid a foundation for the study of vesicle hydrogels. Menger et al. used a gemini surfactant with asymmetric carbon chain length to prepare “necklace” vesicles, and such interesting “pearls on a string” morphology of the vesicles led to the formation of a hydrogel with a network ultrastructure.¹⁵ Raghavan synthesized hydrophobic modified chitosan by which the vesicles formed from cationic surfactant mixtures were joined together to form hydrogels because the hydrophobic chains could be inserted into the bilayers of the vesicles.¹⁶

The morphology of vesicles reported is usually spherical. Nowadays, increasing interest has been paid to polyhedral vesicles that have been found to be formed from some nonionic surfactant systems and cationic surfactant mixtures.^{17,18} However, the hydrogels consisting of polyhedral vesicles have been rarely reported until now.^{19–21} In our previous work, we systematically studied cationic fluoro-/hydrocarbon surfactant mixtures with different alkyl chain lengths and found that hydrogels composed of polyhedral vesicles were formed in certain systems.^{22,23} Therefore, to

Received: March 20, 2024

Revised: May 23, 2024

Accepted: May 24, 2024

Published: June 14, 2024



extend our earlier research about the catanionic fluoro-/hydrocarbon surfactant systems, in this paper, an amphoteric hydrocarbon surfactant, tetradecyl dimethylaminoxide (C_{14} DMAO), was chosen to mix with perfluorinated *n*-nonanoic acid (C_8F_{17} COOH) in an aqueous solution. The phase behavior and rheological properties were investigated. When the total concentration of the two surfactants was fixed, with the mixed ratio changing, a polyhedral vesicle hydrogel was obtained when the C_8F_{17} COOH concentration was higher than the C_{14} DMAO concentration, while rodlike and spherical vesicles formed when the C_{14} DMAO concentration was higher than the C_8F_{17} COOH concentration. This work further proved that the crystalline state of the vesicle bilayers formed by the two surfactants was the main reason for the formation of the polyhedral vesicle hydrogel.

EXPERIMENTAL SECTION

Materials. Perfluorononanoic acid (C_8F_{17} COOH, purity >98%) was purchased from Fluorochem in the United Kingdom. Tetradecyl dimethylaminoxide (30% solution) was purchased from Shanghai Maoming Petrochemical Co. and purified for use. Deionized water (ultrapure water) was purchased from Beijing Maiuida Technology Co., Ltd., and heavy water (D_2O , purity >99.9%) was purchased from Shanghai Civic Chemical Technology Co., Ltd.

Purification of C_{14} DMAO. Appropriate amounts of C_{14} DMAO solution were put in the surface dish, refrigerated for 24 h, and then frozen to be dry in a freeze-dryer for 48 h before taking out. The freeze-dried C_{14} DMAO was added to acetone, which was heated to about 50 °C and stirred until it was completely dissolved. Then, the obtained solution was drained immediately to get the filtrate, which was placed in a surface dish to crystallize naturally. The crystallized samples were refrigerated for 24 h and freeze-dried to obtain a high-purity sample after three repetitions.

Preparation of Samples. Different concentrations of C_{14} DMAO solutions were prepared, and an appropriate amount of C_8F_{17} COOH was added to the C_{14} DMAO solution and fully mixed by shaking with an Aika shaker. After the reaction of the solution was complete, all samples were stored in an incubator at 25.0 ± 0.1 °C and gently shaken by hand every day to accelerate the reaction balance. The balance time was 1 month.

Observation of the Phase Behavior. The phase behavior of the sample was determined by two methods: visual observation and polarizing observation. The method to determine whether the gel-phase sample was formed was mainly by inverting the sample to observe whether the sample flowed. The method to judge the layered phase was to place the sample in the middle of two fully polarized polarizers for observation to see whether it would appear as a color pattern phenomenon.

Textures of the Birefringent Hydrogel and L_α Phase Samples. The birefringent hydrogel and L_α phase samples were characterized on a Carl Zeiss Axioskop 40 light microscope (Jena, Germany) at 25.0 ± 0.1 °C to observe the textures.

Conductivity Measurements. The conductivity was determined by a conductivity meter of model DDSJ-308A and an electrode of model DJS-10C at a constant temperature of 25.0 ± 0.1 °C. The conductivity value of the two-phase system was tested by stirring with magnetons. The final conductivity was the average value after three measurements.

pH Measurements. The pH of the samples was measured by a precision pH meter of model PHS-3C at 25.0 ± 0.1 °C. The two-phase sample was tested by stirring with magnetons.

Freeze-Fracture Transmission Electron Microscopy (FF-TEM) Observations. The etching and copying of the sample were done with a freeze-etched sample maker (EM BAF 060, Leica, Germany). The sample was transferred to the sample chamber of the preparation table, and the temperature was maintained at -150 °C through a liquid nitrogen stream, while the vacuum was controlled at 3×10^{-7} Pa. When the sample temperature reached equilibrium with the cavity temperature, a hard metal knife was used to break the sample bulge, while the temperature was adjusted to briefly etch the ice on the sample surface. Pt/C was then sprayed onto the sample surface at 45° to reproduce the sample structure, and Pt/C was electrospayed onto the sample surface at 90° to support and strengthen the duplicate film. Finally, the replica film was washed and transferred to a bare copper net for drying and was observed by a JEOL JEM-1400 electron microscope at 120 kV. The images were recorded by Gatan 831 CCD ($2.7 \text{ K} \times 2.7 \text{ K}$). All transfer operations were performed in a liquid nitrogen environment (-196 °C).

Cryo-Transmission Electron Microscopy Observations (Cryo-TEM). Cryo-TEM measurements were used to determine the microstructure of the L_α phase samples. About 5 μL of solution was loaded onto a TEM copper grid, which was blotted with two pieces of filter paper to obtain a thin film. After about 4 s to relax any stress induced by the blotting, the sample was instantly frozen by plunging it into liquid ethane (cooled by liquid nitrogen) at -165 °C. Then, the vitrified specimen was inserted into liquid nitrogen and transferred to a cryogenic sample holder (Gatan 626). Finally, a JEOL JEM-1400 electron microscope (120 kV) was used to observe the sample. The images are recorded by a Gatan multiscan CCD.

Differential Scanning Calorimetry (DSC) Measurements. The DSC experiments were performed on a differential scanning calorimeter model DSC-8500 from PerkinElmer. The sample was placed in an aluminum pot, sealed with a nitrogen stream rate of $20 \text{ mL}\cdot\text{min}^{-1}$, and temperature-scanned under this protection at a warming rate of $5 \text{ }^\circ\text{C}\cdot\text{min}^{-1}$, with a scanning range of 10–80 °C. An empty aluminum pot was used for reference.

Wide-Angle X-ray Scattering (WAXS) Measurements. The WAXS measurements were performed by using SAXSess Anton-Paar (Austria) with $\text{Cu K}\alpha$ radiation (0.154 nm) operating at 50 kV and 40 mA. The distance from the samples to the detector was 261 mm, and the temperature was kept at 25.0 ± 0.1 °C.

Small-Angle X-ray Diffraction (XRD) Measurements. The XRD tests of the gel samples were performed on a Shimadzu XRD-6000 X-ray diffractometer. The working conditions were: incident light source, $\text{Cu K}\alpha$ target ($\lambda = 1.5418 \text{ \AA}$); voltage, 40 kV; current, 40 mA; scanning speed, $1^\circ\cdot\text{min}^{-1}$; recording angle, 1–10° (small angle). MDI Jade 6 software was used for data processing.

^1H Nuclear Magnetic Resonance (^1H NMR) Measurements. ^1H NMR experiments were performed on a Bruker AVANCE 400 Meg NMR instrument using a pulsed field gradient module (Z-axis) and a 5 mm BBO probe. The operating temperature was controlled at 25.0 ± 0.1 °C.

Rheological Property Measurements. The Z41 Ti coaxial rotary measuring system was used for nongel samples, and the non-slip PP20 laminae measuring system was used for

hydrogel samples. The curves of the energy storage modulus (G') and loss modulus (G'') with angular frequency were measured (the scanning frequency range was 0.01–10.0 Hz), and the curves of G' and G'' with shear stress were also measured (the shear rate range was 0.001–1000 s^{-1}). The scanning range was 0.001–20.0 Pa, and the test operating temperature was 25.0 ± 0.1 °C.

RESULTS AND DISCUSSION

Phase Behavior of $C_8F_{17}COOH/C_{14}DMAO/H_2O$. Figure 1 shows the phase diagram of the $C_8F_{17}COOH/C_{14}DMAO/H_2O$

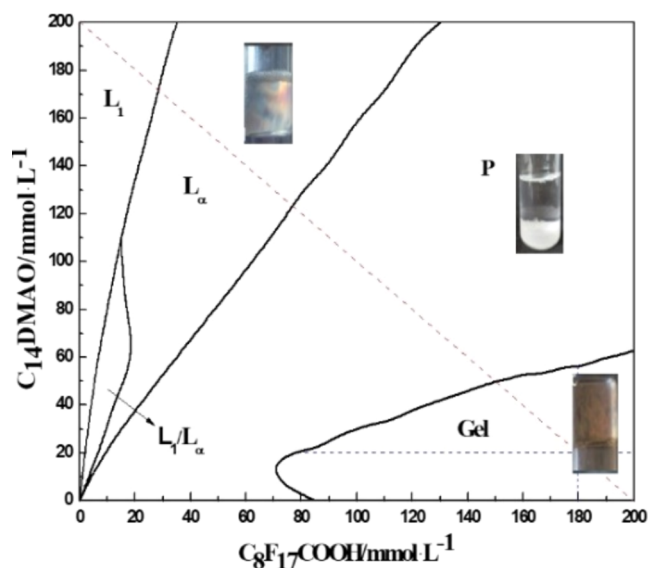


Figure 1. Phase diagram of the $C_8F_{17}COOH/C_{14}DMAO/H_2O$ system at 25 ± 0.1 °C. The pictures of the gel phase and L_α phase under the polarized film were also shown in the corresponding regions.

H_2O system at 25 °C, in which the concentrations of both surfactants ranged from 0 to 200 $mmol \cdot L^{-1}$. As shown in Figure 1, the system showed very rich phase behavior, and the phase diagram was divided into five regions. When the content of $C_8F_{17}COOH$ was high and the content of $C_{14}DMAO$ was low, the bottom right corner of the phase diagram was the gel region. The hydrogel sample in this region was clear and transparent in appearance, and a distinct multicolored pattern was observed under the polarizer. Besides, as revealed in Figure 2a, the typical gel sample with 160 $mmol \cdot L^{-1}$ $C_8F_{17}COOH$ and 40 $mmol \cdot L^{-1}$ $C_{14}DMAO$ showed stripe textures under a polarizing microscope, which demonstrated the existence of

the lamellar phase (the L_α phase). As the amount of $C_{14}DMAO$ increased, a large area of the precipitate was observed in the phase diagram. With the further increase of the content of $C_{14}DMAO$, the appearance of the sample appeared light blue, and very obvious colorful patterns were seen when observed through polarizers. This area was also the L_α phase, which was further proved by the crosslike spherulite textures (Figure 2b) of the selected sample with 40 $mmol \cdot L^{-1}$ $C_8F_{17}COOH$ and 160 $mmol \cdot L^{-1}$ $C_{14}DMAO$. When the content of $C_{14}DMAO$ was high and the content of $C_8F_{17}COOH$ was low, the appearance of the sample was clear and transparent with good fluidity. The isotropic L_1 phase in this region was a micellar phase. In addition, there was a small range of the L_1/L_α two-phase coexistence zone, where the upper part was the L_1 phase and the lower part was the L_α phase, indicating that the density of the L_α phase was greater than that of the L_1 phase.

In order to study the phase behavior of this system more accurately, the diagonal line in the phase diagram, that is, the total concentration of the system solution was 200 $mmol \cdot L^{-1}$, and the mixed ratio of the two surfactants ($r = n_{C_{14}DMAO}/n_{C_8F_{17}COOH}$) was changed, and it was chosen for further study. The results are shown in Figure 3, including the conductivity and pH values of the samples. As can be seen from Figure 3, when the concentration of $C_{14}DMAO$ ranged from 0 to 50 $mmol \cdot L^{-1}$, a birefringent hydrogel phase was observed, a typical sample of which is shown in Figure 1. FF-TEM measurements showed that interesting monolayer polyhedral vesicles and spherical vesicles were formed in the hydrogel phase, as shown in Figure 4a, in which the vertices and edges of the polyhedron were clearly visible. When the concentration of $C_{14}DMAO$ ranged from 50 to 122 $mmol \cdot L^{-1}$, the system presented a precipitated phase, which might be due to the mutual repulsion of carbon and fluorine chains, leading to macroscopic phase separation in the system. When the concentration of $C_{14}DMAO$ was 122–170 $mmol \cdot L^{-1}$, the solution was in the L_α phase, and a typical sample of this region is shown in Figure 1. Unlike the hydrogel phase, monolayer spherical vesicles, rod vesicles, and some elongated vesicles were found to be formed in the L_α phase samples (Figure 4b), which were much smaller in size than the vesicles of the hydrogel phase. The L_1 micellar phase was observed by increasing the concentration of $C_{14}DMAO$. In addition, it was observed from Figure 3a that with the increase of $C_{14}DMAO$ content, the pH value of the system gradually increased, which was due to the neutralization of acid by weakly alkaline $C_{14}DMAO$. The conductivity test results in Figure 3b showed that the conductivity of the hydrogel phase and the L_α phase

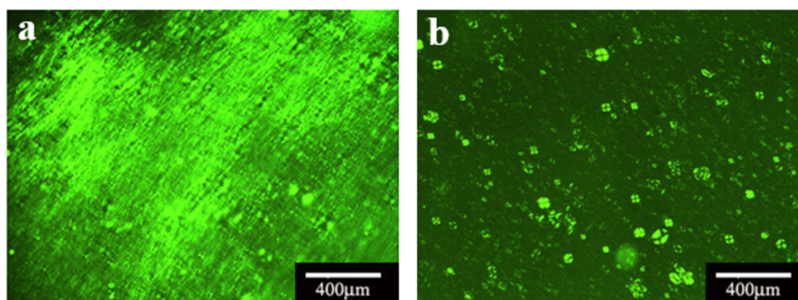


Figure 2. Polarized textures of two birefringent samples: (a) the gel phase with 160 $mmol \cdot L^{-1}$ $C_8F_{17}COOH$ and 40 $mmol \cdot L^{-1}$ $C_{14}DMAO$ and (b) the L_α phase with 40 $mmol \cdot L^{-1}$ $C_8F_{17}COOH$ and 160 $mmol \cdot L^{-1}$ $C_{14}DMAO$.

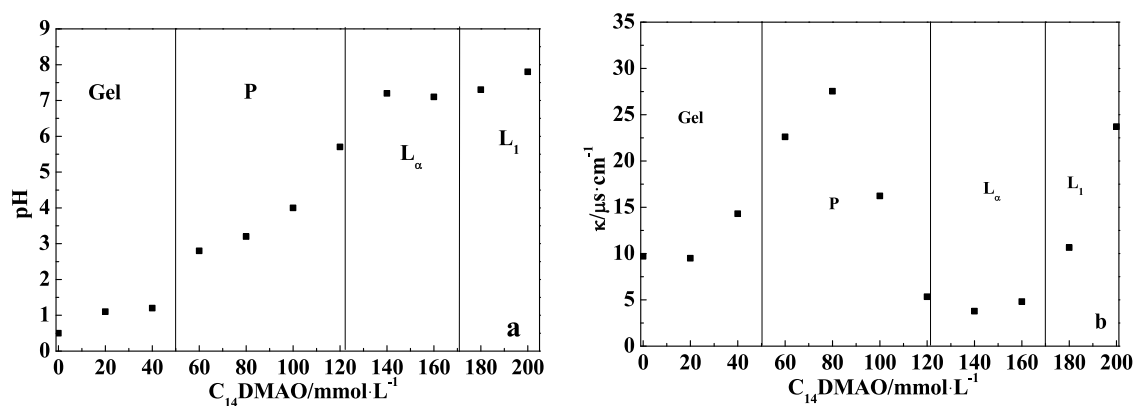


Figure 3. (a) Conductivity and (b) pH values of the $C_8F_{17}COOH/C_{14}DMAO/H_2O$ system. $c_T = 200 \text{ mmol}\cdot\text{L}^{-1}$. $T = 25 \pm 0.1 \text{ }^\circ\text{C}$.

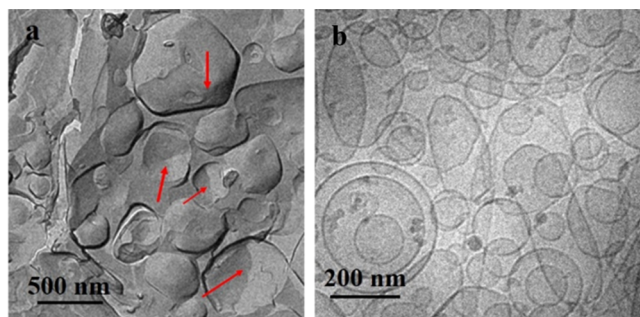


Figure 4. (a) FF-TEM picture of the gel phase with $160 \text{ mmol}\cdot\text{L}^{-1}$ $C_8F_{17}COOH$ and $40 \text{ mmol}\cdot\text{L}^{-1}$ $C_{14}DMAO$ and (b) cryo-TEM picture of the L_α phase with $40 \text{ mmol}\cdot\text{L}^{-1}$ $C_8F_{17}COOH$ and $160 \text{ mmol}\cdot\text{L}^{-1}$ $C_{14}DMAO$.

was lower than that of the samples in the adjacent phase region because the vesicles formed in these two regions could cover some conductive ions.

Phase Transition Temperature. Differential scanning calorimetry (DSC) can be used to characterize the states of surfactant bilayers of the hydrogel phase and the L_α phase. As shown in Figure 5, the presence of phase transition temperature was observed when the hydrogel samples were heated, indicating that the bilayer films had a transition process from the crystalline state to the liquid state. In addition, it was also observed that when $20 \text{ mmol}\cdot\text{L}^{-1}$ $C_{14}DMAO$ was added to a $180 \text{ mmol}\cdot\text{L}^{-1}$ $C_8F_{17}COOH$ solution, the phase transition

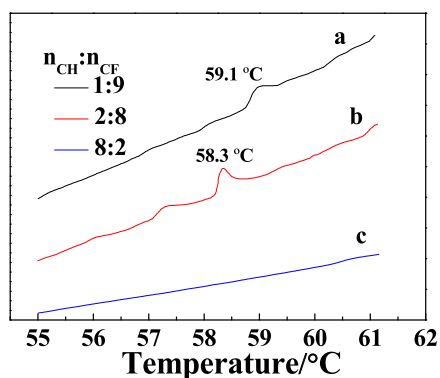


Figure 5. DSC curves of the typical samples with different mixed ratios of $C_{14}DMAO$ and $C_8F_{17}COOH$ (n_{CH}/n_{CF}): (a) 1:9, (b) 2:8, and (c) 8:2. $c_T = 200 \text{ mmol}\cdot\text{L}^{-1}$.

temperature of the hydrogel sample was $59.1 \text{ }^\circ\text{C}$. The phase transition temperature increased relative to the Krafft point of $C_8F_{17}COOH$ ($48.3 \text{ }^\circ\text{C}^{22}$). When $40 \text{ mmol}\cdot\text{L}^{-1}$ $C_{14}DMAO$ was added to a $160 \text{ mmol}\cdot\text{L}^{-1}$ $C_8F_{17}COOH$ solution, the phase transition temperature of the hydrogel sample was $58.3 \text{ }^\circ\text{C}$. When the $C_{14}DMAO$ concentration was increased to $160 \text{ mmol}\cdot\text{L}^{-1}$, the phase transition temperature disappeared. Apparently, the phase transition temperature of the samples decreased as the $C_{14}DMAO$ concentration was increased. This was because the fluorocarbon chain was rigid and had a high chain melting temperature, while the $C_{14}DMAOH^+$ chain was soft and its chain transformation temperature was lower than room temperature, so in this system, the transformation process of the vesicle bilayer from the crystal state to the liquid state was mainly caused by the melting of the $C_8F_{17}COO^-$ chain when heated. Therefore, the phase transition temperature obtained by DSC was mainly the result of the synergistic effect of the following two factors: one was the electrostatic interaction between the $C_8F_{17}COO^-$ chain and the $C_{14}DMAOH^+$ chain, which led to the increase of the chain melting temperature, and another factor was the cocrystallization of the $C_8F_{17}COO^-$ chain and the $C_{14}DMAOH^+$ chain. The phase transition temperature of the $C_{14}DMAOH^+$ chain was lower than room temperature, so this cocrystallization would lead to the reduction of the chain transition temperature. When a small amount of $C_{14}DMAOH^+$ was added, electrostatic interaction occurred between the $C_8F_{17}COO^-$ chain and the $C_{14}DMAOH^+$ chain, thus making the phase transition temperature higher than the Krafft point of the $C_8F_{17}COO^-$ chain, as shown in curves a and b in Figure 5. However, when the concentration of $C_{14}DMAO$ increased, the cocrystallization of the $C_8F_{17}COO^-$ chain and $C_{14}DMAOH^+$ chain played a dominant role, so the phase transition temperature disappeared, as shown in curve c of Figure 5. For the sample of $40 \text{ mmol}\cdot\text{L}^{-1}$ $C_8F_{17}COOH/160 \text{ mmol}\cdot\text{L}^{-1}$ $C_{14}DMAO$, no phase transition occurred in the studied temperature range (Figure 5c), indicating that the bilayer of spherical and rod-shaped vesicles was in the liquid state, which was consistent with the results observed by FF-TEM (Figure 4b). It was because of the “flexibility” of the bilayers that some spherical vesicles were elongated into ellipsoids. The hydrogel system was more inclined to form polyhedral vesicles because the bilayer was in the crystalline state and the rigidity was relatively strong.

Layer Spacing of the Hydrogel Phase. In order to obtain more information on the hydrogel phase, XRD measurements were performed for the typical sample with 40

mmol·L⁻¹ C₁₄DMAO and 160 mmol·L⁻¹ C₈F₁₇COOH, and the result is shown in Figure 6. From Figure 6, it was seen that

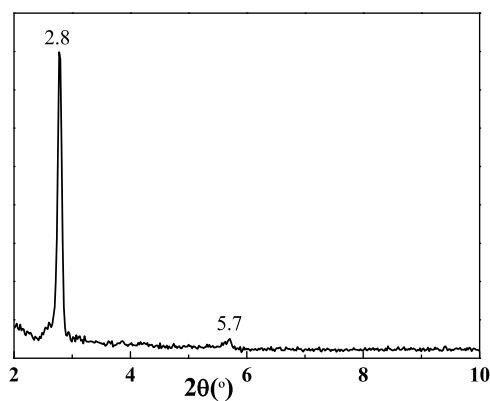


Figure 6. XRD curves of the hydrogel sample with 160 mmol/L C₈F₁₇COOH and 40 mmol/L C₁₄DMAO.

the hydrogel phase had two well-resolved reflection peaks at 2.8 and 5.7°, and the corresponding diffraction factor q values of these two peaks were 2.0 and 4.0, respectively. The ratio of q_1/q_2 was 1:2, indicating that the hydrogel had high crystallinity, which was highly consistent with the DSC results. The crystal structure was layered, and the layer spacing d was 3.2 nm, calculated by the Bragg equation. Furthermore, the d value of 3.2 nm was a little less than twice as long as the chain length of the C₁₄DMAO molecules (3.8 nm), which belonged to the combination of two C₁₄DMAO molecules through hydrophobic interaction in each unit of the arrays.^{24,25}

WAXS Measurements. The selected hydrogel sample with 160 mmol/L C₈F₁₇COOH and 40 mmol/L C₁₄DMAO at different temperatures was further investigated by WAXS measurements, and the results are shown in Figure 7. The

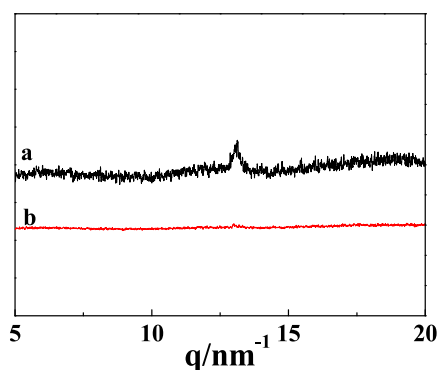


Figure 7. WAXS curves of the hydrogel sample with 160 mmol/L C₈F₁₇COOH and 40 mmol/L C₁₄DMAO at 25 ± 0.1 °C (a) and 60 ± 0.1 °C (b) respectively.

pattern of the hydrogel sample presented a single, sharp peak at 13.1 nm⁻¹ (Figure 7a) at room temperature, which was characteristic of the surfactant chains in the crystalline state with a local in-plane orthorhombic packing spatially averaged into hexagonal packing.^{26–28} However, no peak was seen from the pattern of the hydrogel sample at 60 °C, as shown in Figure 7b, indicating that the surfactant chains of the sample were in the liquid state when the temperature was higher than the phase transition temperature (58.3 °C). The WAXS results were consistent with the results of DSC measurements.

¹H NMR Results. In order to better understand the formation of the polyhedral vesicle hydrogel, we further characterized the hydrogel phase by ¹H NMR. Figure 8 shows

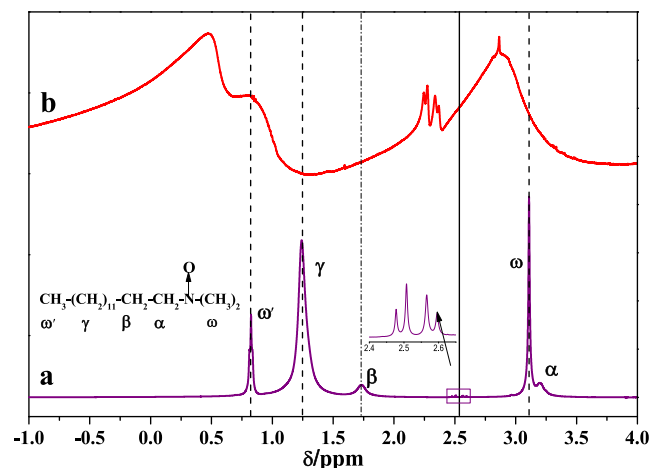


Figure 8. ¹H NMR curves of two samples: (a) 40 mmol·L⁻¹ C₁₄DMAO solution and (b) the hydrogel phase with 160 mmol·L⁻¹ C₈F₁₇COOH and 40 mmol·L⁻¹ C₁₄DMAO.

the ¹H NMR curves of the 40.00 mmol·L⁻¹ C₁₄DMAO solution and the hydrogel containing 40 mmol·L⁻¹ C₁₄DMAO and 160 mmol·L⁻¹ C₈F₁₇COOH. When C₈F₁₇COOH was not added, the C₁₄DMAO molecular chains in the C₁₄DMAO solution could flow freely, thus making the ¹H NMR signals of different groups on the carbon chains very strong and the signal peaks very sharp, as shown in Figure 8a. However, as shown in Figure 8b, it was found that when the fluorocarbon surfactant was added to the system, the chemical shift of the hydrogen spectrum of C₁₄DMAO moved to a low field. Meanwhile, the peak width formed became significantly wider, and the signal peak became weaker. Especially α -CH₂ and β -CH₂ peaks disappeared, which was because in the gel phase, the fluidity of the C₁₄DMAO monomer was limited, so the ¹H NMR signal became difficult to distinguish and the signal peak became weak. At the same time, it also showed that C₁₄DMAO, after being protonated by C₈F₁₇COOH, had a great influence on hydrogen in these positions, which proved the existence of hydrogen bonds in the system. Therefore, it could be concluded that the driving force of vesicle formation was not only the electrostatic interaction between cationic and anionic ions and the interaction between C–H and C–F chains but also the intermolecular hydrogen bond.

Formation Mechanism of the Vesicle Hydrogel. Based on the above results, the formation mechanism of the vesicle hydrogel was proposed, as shown in Scheme 1. The sample preparation in the C₈F₁₇COOH/C₁₄DMAO system was only done by heating at 60 °C to facilitate C₈F₁₇COOH dissolution and cooling at 25 °C to achieve phase equilibrium. Therefore, no additional energy was introduced, thus ensuring that the shape of the vesicle was determined only by the intermolecular forces. Besides, the DSC and WAXS results proved the crystallization state of the bilayers of the polyhedral vesicles, which demonstrated that the formation of the polyhedral vesicles was driven by the recrystallization of the two kinds of surfactants.²⁹ The formation of the polyhedral vesicles is presented in Scheme 1. Perfluorooctanoic acid dissolved in an aqueous solution was easily ionized to form C₈F₁₇COO⁻.

Scheme 1. Schematic Representation of the Polyhedral Vesicle Formed from the Self-assembly of the $C_8F_{17}COOH@C_{14}DMAO$ Complexes in an Aqueous Solution

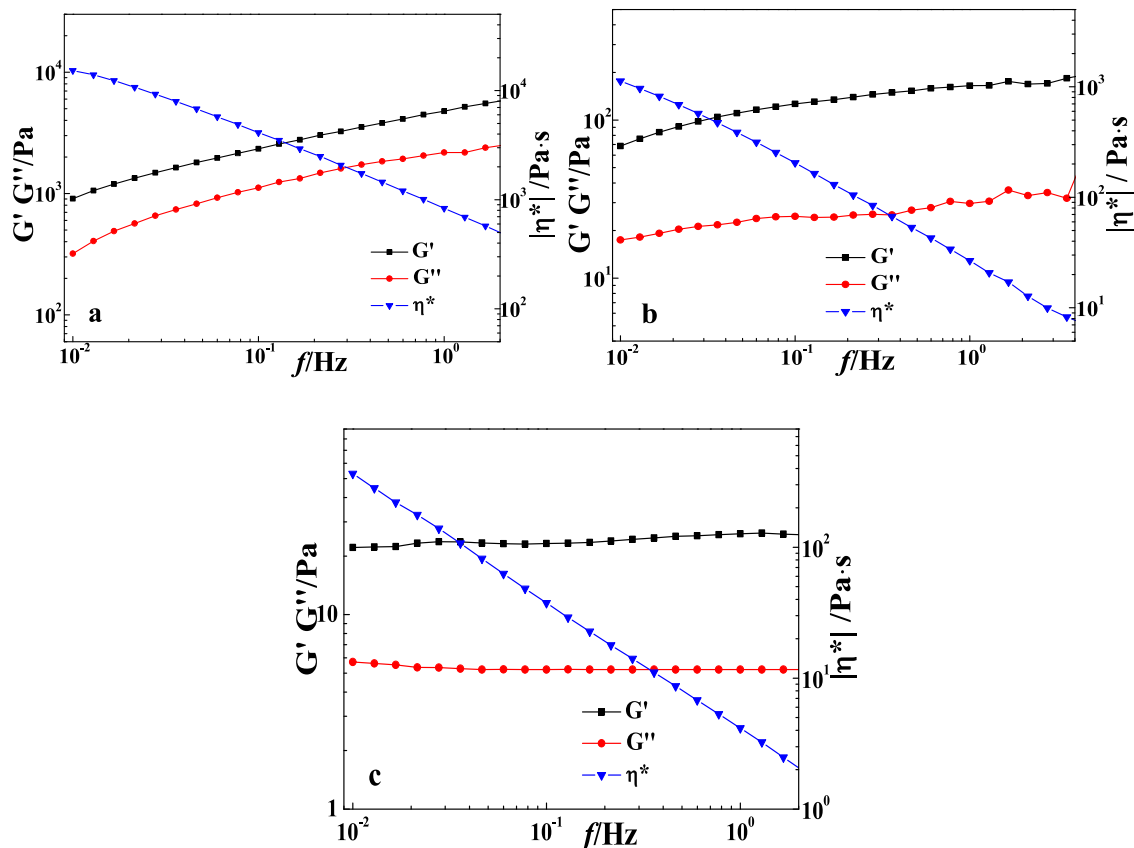
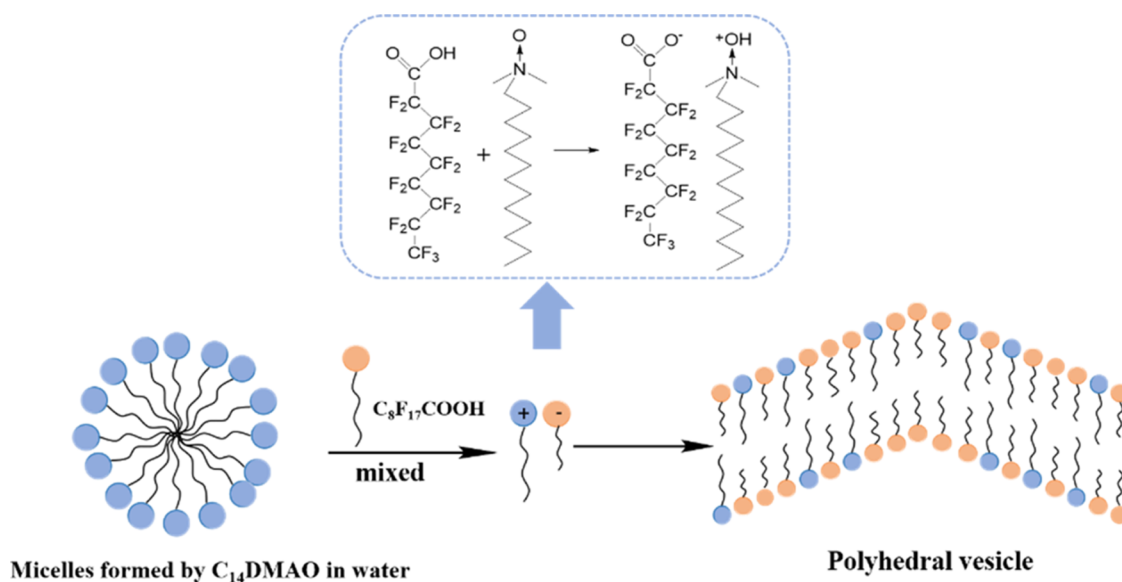


Figure 9. Oscillatory rheological results of the typical samples with different r : (a) 1:9, (b) 2:8, and (c) 8:2. $c_T = 200 \text{ mmol}\cdot\text{L}^{-1}$.

When $C_8F_{17}COOH$ was added to the $C_{14}DMAO$ solution, $C_8F_{17}COOH$ was inserted into the monolayer of the $C_{14}DMAO$ micelle. In the mixtures, the $C_8F_{17}COOH$ molecules protonated $C_{14}DMAO$ molecules with the carboxyl group to form $C_{14}DMAOH^+ \cdots C_8F_{17}COO^-$ ion pairs. When the solution was cooled from 60°C to room temperature, the hydrocarbon–fluorocarbon chain crystallized into a solid state, while the ionized $C_8F_{17}COO^-$ aggregated to form the apex of

the polyhedral vesicle, and $C_{14}DMAOH^+$ was randomly embedded in the bilayer of the polyhedral vesicle to form an ion pair with $C_8F_{17}COO^-$ (Scheme 1). Polyhedral vesicles were then densely packed to form hydrogels.

Rheological Properties of the Polyhedral Vesicle Hydrogel. Figure 9 shows the shear rheological test results of three typical samples. The elastic modulus G' and the viscous modulus G'' of the samples decreased with the

C14DMAO concentration. Besides, it was seen from Figure 9a,b that the elastic modulus G' and the viscous modulus G'' of the hydrogel samples were both very high, and the elastic modulus was higher than the viscous modulus within the measured range. The composite viscosity decreased linearly with the increase of frequency, which indicated that it had great viscoelasticity. At the same time, both the elastic modulus and viscous modulus increased with the increase of frequency, and the amplitude of the increase remained the same, which was a typical rheological property of the hydrogel phase. The rheological properties of L_α phase samples were different from those of the gel-phase samples. As shown in Figure 9c, the elastic modulus and viscosity modulus of L_α phase samples hardly change with the change in frequency, and their values were also much smaller than those of the gel-phase samples. A similar phenomenon can also be observed in the steady shear results shown in Figure 10. The apparent viscosity also

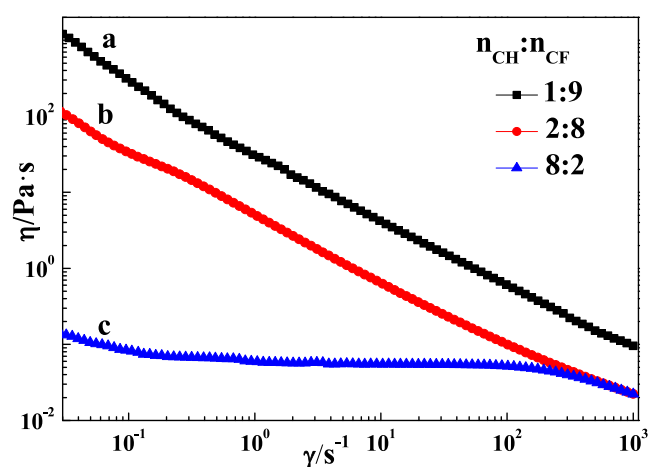


Figure 10. Steady shear rheograms of the selected samples with different r : (a) 1:9, (b) 2:8, and (c) 8:2. $c_T = 200 \text{ mmol}\cdot\text{L}^{-1}$.

decreased with increasing C14DMAO concentration. The samples with $n_{\text{CH}}/n_{\text{CF}} = 1:9$ and $2:8$ behaved strongly with shear thinning with increasing shear rate, which was the gel-like character. Differently, the apparent viscosity of the sample with $n_{\text{CH}}/n_{\text{CF}} = 8:2$ remained almost unchanged over the full range of shear rates with a viscosity of around $0.06 \text{ Pa}\cdot\text{s}$.

In order to further study the factors affecting the rheological properties of the hydrogel phase, a series of hydrogel samples

were obtained by fixing the concentration of the cationic surfactant in the gel phase and changing the concentration of another one, and the rheological properties were determined. The stress scanning curves of different samples are shown in Figure 11. Figure 11a shows the elastic modulus stress-scan curve obtained by changing the concentration of $\text{C}_8\text{F}_{17}\text{COOH}$ with a fixed concentration of C_{14}DMAO of $20 \text{ mmol}\cdot\text{L}^{-1}$, and Figure 11b shows the elastic modulus obtained by changing the concentration of C_{14}DMAO with a fixed concentration of $\text{C}_8\text{F}_{17}\text{COOH}$ of $180 \text{ mmol}\cdot\text{L}^{-1}$. As could be seen from Figure 11, when the stress increased, obvious yield values were observed, and the yield stress could be intuitively compared from the figure. When the C_{14}DMAO concentration was fixed and the concentration of $\text{C}_8\text{F}_{17}\text{COOH}$ was changed, the yield stress showed an obvious rise with the increase in concentration (Figure 11a). However, when the $\text{C}_8\text{F}_{17}\text{COOH}$ concentration was unchangeable but the C_{14}DMAO concentration was changed, the yield stress did not change significantly. This fully showed that the viscoelasticity of such vesicle gels was mainly determined by fluorocarbon surfactants. Due to the strong rigidity of fluorocarbon chains, changing the content of fluorocarbon chains would have a great impact on the rheological properties of the hydrogels.

CONCLUSIONS

The $\text{C}_8\text{F}_{17}\text{COOH}/\text{C}_{14}\text{DMAO}$ mixed system studied in this article had rich phase behavior and novel aggregation properties in an aqueous solution. Interestingly, the hydrogels consisting of both polyhedral and spherical vesicles were successfully constructed in this system, and the bilayer film was in a crystalline state at room temperature. Therefore, the formation of polyhedral vesicles in this system was caused by the cocrystallization of $\text{C}_8\text{F}_{17}\text{COO}^-$ and $\text{C}_{14}\text{DMAOH}^+$ chains in the bilayer. The rheological results showed that the vesicle hydrogels had great viscoelasticity, and the viscoelasticity was mainly determined by the content of $\text{C}_8\text{F}_{17}\text{COOH}$. This work is of great significance in explaining the formation mechanism of vesicle hydrogels and expanding the application of such hydrogels in various fields.

AUTHOR INFORMATION

Corresponding Author

Juan Zhang – State Key Laboratory of Shale Oil and Gas Enrichment Mechanisms and Effective Development,

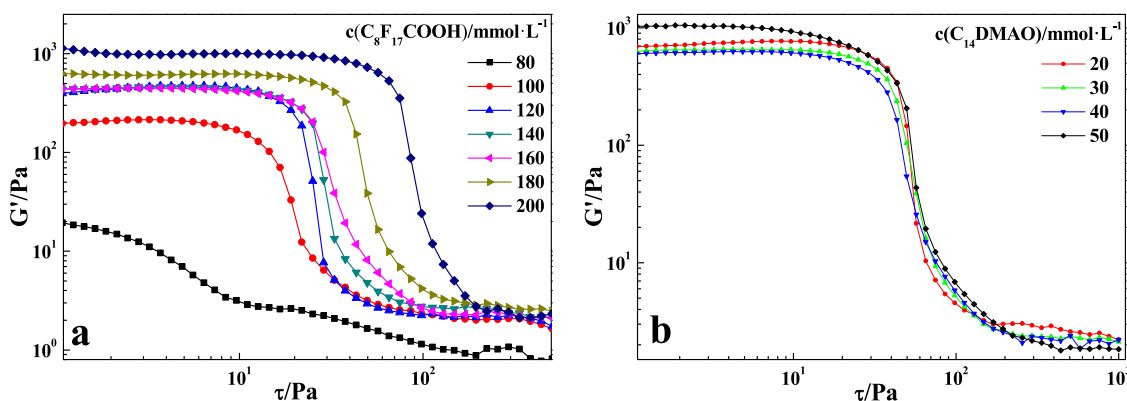


Figure 11. G' as a function of oscillatory stress at different proportions: (a) $20 \text{ mmol}\cdot\text{L}^{-1}$ C_{14}DMAO with different concentrations of the $\text{C}_8\text{F}_{17}\text{COOH}$ solution and (b) $180 \text{ mmol}\cdot\text{L}^{-1}$ $\text{C}_8\text{F}_{17}\text{COOH}$ with different concentrations of the C_{14}DMAO solution. $T = 25 \pm 0.1 \text{ }^\circ\text{C}$.

SINOPEC Exploration and Production Research Institute, Beijing 102206, P. R. China; Research and Development Center for the Sustainable Development of Continental Sandstone Mature Oilfield by National Energy Administration, SINOPEC Exploration and Production Research Institute, Beijing 102206, P. R. China; Unconventional Petroleum Research Institute, China University of Petroleum, Beijing 102249, P. R. China; orcid.org/0000-0002-9247-4371; Phone: +86-010-89733077; Email: juanzhang@cup.edu.cn

Authors

Ping Liu – State Key Laboratory of Shale Oil and Gas Enrichment Mechanisms and Effective Development, SINOPEC Exploration and Production Research Institute, Beijing 102206, P. R. China; Research and Development Center for the Sustainable Development of Continental Sandstone Mature Oilfield by National Energy Administration, SINOPEC Exploration and Production Research Institute, Beijing 102206, P. R. China

Yuan Gao – Unconventional Petroleum Research Institute, China University of Petroleum, Beijing 102249, P. R. China

Qichao Lv – Unconventional Petroleum Research Institute, China University of Petroleum, Beijing 102249, P. R. China; orcid.org/0000-0002-3270-5684

Denglai Wu – Unconventional Petroleum Research Institute, China University of Petroleum, Beijing 102249, P. R. China

Yi Tian – Unconventional Petroleum Research Institute, China University of Petroleum, Beijing 102249, P. R. China

Jigui Tang – Unconventional Petroleum Research Institute, China University of Petroleum, Beijing 102249, P. R. China

Complete contact information is available at:

<https://pubs.acs.org/10.1021/acsomega.4c02696>

Notes

The authors declare no competing financial interest.

ACKNOWLEDGMENTS

This research is supported by the open fund project of Research and Development Center for the Sustainable Development of Continental Sandstone Mature Oilfield by National Energy Administration (No. 33550000-22-ZC0613-0221).

REFERENCES

- (1) Whitesides, G. M.; Grzybowski, B. Self-assembly at all scales. *Science* **2002**, *295*, 2418.
- (2) Moore, J. S.; Kraft, M. L. Synchronized self-assembly. *Science* **2008**, *320*, 620.
- (3) Pietrasik, J.; Vamvakaki, M.; Padnya, P. Editorial: Self-assembly as a tool for functional materials design. *Front. Chem.* **2002**, *10*, No. 1010285, DOI: [10.3389/fchem.2022.1010285](https://doi.org/10.3389/fchem.2022.1010285).
- (4) Diao, H.; Lu, Y. H.; Ling, Y.; Shen, Y. J.; Yu, J. M.; Ma, K. Peptide-based self-assembly: design, bioactive properties, and its applications. *Curr. Pharm. Des.* **2023**, *29*, 640.
- (5) Benoit, R. M.; Frey, D.; Hilbert, M.; et al. Structural basis for recognition of synaptic vesicle protein 2C by botulinum neurotoxin A. *Nature* **2014**, *505*, 108.
- (6) Liu, J.; He, P. L.; Yan, J. L.; et al. An organometallic super-gelator with multiple-stimulus responsive properties. *Adv. Mater.* **2008**, *20*, 2508.
- (7) Lin, Y. Y.; Cheng, X. H.; Qiao, Y.; et al. Creation of photo-modulated multi-state and multi-scale molecular assemblies via binary-state molecular switch. *Soft Matter* **2010**, *6*, 902.

- (8) Jiang, L. X.; Wang, K.; Ke, F. Y.; et al. Endowing cationic surfactant vesicles with dual responsive abilities via a noncovalent strategy: introduction of a responder, sodium cholate. *Soft Matter* **2009**, *5*, 599.

- (9) Roig, F.; Blanzat, M.; Solans, C.; et al. Hyaluronan based materials with cationic sugar-derived surfactants as drug delivery systems. *Colloids Surf., B* **2018**, *164*, 218.

- (10) Lee, J. H.; Oh, H.; Baxa, U.; et al. Biopolymer-connected liposome networks as injectable materials capable of sustained drug delivery. *Biomacromolecules* **2012**, *13*, 3388.

- (11) Hao, X.; Liu, H.; Xie, Y. J.; et al. Thermal-responsive self-healing hydrogel based on hydrophobically modified chitosan and vesicle. *Colloid Polym. Sci.* **2013**, *291*, 1749.

- (12) Minkenberg, C. B.; Hendriksen, W. E.; Li, F.; et al. Dynamic covalent assembly of stimuli responsive vesicle gels. *Chem. Commun.* **2012**, *48*, 9837.

- (13) Marianecchi, C.; Carafa, M.; Marzio, L. D.; et al. A new vesicle-loaded hydrogel system suitable for topical applications: Preparation and characterization. *J. Pharm. Pharm. Sci.* **2011**, *14*, 336.

- (14) Gradzielski, M.; Bergmeier, M.; Muller, M.; Hoffmann, H. Novel gel phase: A cubic phase of densely packed monodisperse, unilamellar vesicles. *J. Phys. Chem. B* **1997**, *101*, 1719.

- (15) Lee, J. H.; Gustin, J. P.; Chen, T. H.; et al. Vesicle-biopolymer gels: networks of surfactant vesicles connected by associating biopolymers. *Langmuir* **2005**, *21*, 26.

- (16) Nasser, B.; Florence, A. T. Some properties of extruded non-ionic surfactant micro-tubes. *Int. J. Pharm.* **2003**, *254*, 11.

- (17) Bernheim-Grosswasser, A.; Ugazio, S.; Gauffre, F.; et al. Spherulites: A new vesicular system with promising applications. An example: Enzyme microencapsulation. *J. Chem. Phys.* **2000**, *112*, 3424.

- (18) Lootens, D.; Vautrin, C.; Van Damme, H.; Damme, H. V. Faceted hollow silica vesicles made by templating cationic surfactant vesicles. *J. Mater. Chem.* **2003**, *13*, 2072.

- (19) González-Pérez, A.; Schmutz, M.; Waton, G.; et al. Isolated fluid polyhedral vesicles. *J. Am. Chem. Soc.* **2007**, *129*, 756.

- (20) Jung, H. T.; Lee, S. Y.; Kaler, E. W.; et al. Gaussian curvature and the equilibrium among bilayer cylinders, spheres, and discs. *Proc. Natl. Acad. Sci. U.S.A.* **2002**, *99*, 15318.

- (21) Zhang, J.; Song, A.; Li, Z.; et al. Phase behavior and self-assembly properties of two cationic surfactant systems: C₈F₁₇COOH/TTAOH/H₂O and C₈H₁₇COOH/TTAOH/H₂O. *J. Phys. Chem. B* **2010**, *114*, 13128.

- (22) Zhang, J.; Xu, G. Y.; Zhou, Y. X.; et al. Polyhedral vesicles with crystalline bilayers formed from cationic mixtures of fluorocarbon and hydrocarbon amphiphiles. *J. Colloid Interface Sci.* **2013**, *407*, 318.

- (23) Zhang, J.; Yang, Z. H.; Zhang, H. S.; et al. Hydrogels consisting of vesicles constructed via the self-assembly of a supermolecular complex formed from α -cyclodextrin and perfluorononanoic acid. *Langmuir* **2019**, *35*, 16893.

- (24) Song, S. S.; Feng, L.; Song, A. X.; Hao, J. Room-temperature super hydrogel as dye adsorption agent. *J. Phys. Chem. B* **2012**, *116*, 12850.

- (25) Regev, O.; Guillemet, F. Various bilayer organizations in a single-tail nonionic surfactant: Unilamellar vesicles, multilamellar vesicles, and flat-stacked lamellae. *Langmuir* **1999**, *15*, 4357.

- (26) Cocquyt, J.; Olsson, U.; Olofsson, G.; der Meeren, P. V. Temperature quenched DODAB dispersions: Fluid and solid state coexistence and complex formation with oppositely charged surfactant. *Langmuir* **2004**, *20*, 3906.

- (27) Lohner, K.; Latal, A.; Degovics, G.; Garidel, P. Packing characteristics of a model system mimicking cytoplasmic bacterial membranes. *Chem. Phys. Lipids* **2001**, *111*, 177.

- (28) Zemb, T.; Carrière, D.; Glinel, K.; Hartman, M.; et al. Cationic bilayers as micro-crystals with in-plane ordered alternated charges. *Colloids Surf., A* **2007**, *303*, 37.

- (29) Zemb, T.; Dubois, M.; Demé, B.; Gulik-Krzywicki, T. Self-assembly of flat nanodiscs in salt-free cationic surfactant solutions. *Science* **1999**, *283*, 816.